Electronic Supplementary Material (ESI) for ChemComm.
This journal is © The Royal Society of Chemistry 2023

Supporting Information

High efficiency carbon dot above 60% with both delayed fluorescence and room-temperature phosphorescence

Bin Xu [a #], Qun Hao [b, c #], Xin Tang [a, c] and Menglu Chen [a, b, c*]

A School of Optics and Photonics, Beijing Institute of Technology, Beijing 100081, China.

B Physics Department, Changchun University of Science and Technology, Changchun, 130022

C Yangtze Delta Region Academy of Beijing Institute of Technology, Jiaxing 314019, China.

* *Corresponding author:* menglu@bit.edu.cn

Experimental Section

Materials and Synthesis

Materials. Ethanol anhydrous and ethylene glycol were purchased from Aladdin Chemicals. 1,3-Propanediamine and Polyphosphoric acid were obtained from Shanghai Macklin Biochemical Co. Ltd. Deionized water was used in the experiments. Sulfuric acid purchased from Sinopharm Group Chemical Reagent Co.

Characterization Method. Transmission electron microscopy (TEM, JEOL JEM 2100) was used to measure the morphology of CDs. Atomic force microscopy (AFM) images and X-ray powder diffraction pattern (XRD) were performed using MultiMode V SPM and X-ray diffraction (PANalytical X'Pert Pro MPD), respectively. Optical absorption spectra and steady/transient-state photoluminescence spectra were measured with UV spectrophotometry (UV-2600) and Edinburgh spectrometry (FLS1000), respectively. Fourier transforms infrared (FTIR) spectrum was performed using a Nicolet spectrograph. X-ray photoelectron spectra (XPS) and Raman spectra were recorded using electron spectrometry (ESCALab220i-XL) and Raman spectroscopy (LabRAM Aramis). TGA was recorded from a TA Instruments Q50 thermal analyzer (New Castle, DE, USA) under a stream of nitrogen (N_2) gas with a heating rate of 5 °C min^{-1}. Differential scanning calorimetry (DSC) was studied using a TA Q20 differential scanning calorimeter with a scan rate of 5 °C min^{-1}.

Measurement of RTP Quantum Yield. The absolute photoluminescence quantum yields (PLQY) of all compounds in the solid state were measured using an Edinburgh FLS1000 with an integrating sphere under ambient conditions. The PLQY of all samples were obtained following the equation where A and B represent the integral areas of total photoluminescence (PL) spectra and phosphorescence spectra, respectively. The phosphorescence was separated from the total PL spectrum on the basis of the phosphorescence spectrum for phosphorescence quantum yields.

$$\phi_{RTP} = \frac{B}{A} \times \phi_{PL}$$

Synthesis of NP-CDs$_{1h}$, NP-CDs$_{3h}$ and NP-CDs$_{6h}$. In a typical process, 1,3-propanediamine (1.0 mL) and polyphosphoric acid (1.0 g) were dissolved in ethanol anhydrous (20 mL) to form a clear dispersion. The resultant dispersion was transferred to a beaker (50 mL), heated at 200 ºC for 6.0 h, and then naturally cooled down to room temperature. Yellow solution were formed during the cooling process. Finally, the NP-CDs was obtained by dialyzing with a dialysis membrane (MWC: 500 Da) for 2 days, respectively. NP-CDs were further heated at 200°C for 1h, 3h, and 6h, respectively, the NP-CDs$_{1h}$, NP-CDs$_{3h}$ and NP-CDs$_{6h}$ were obtained, respectively

Results and Discussion

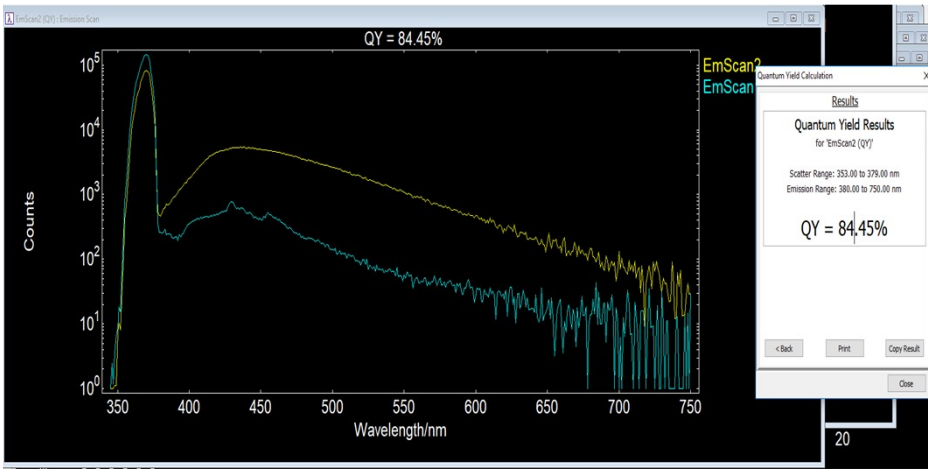

Fig. S1. The photoluminescence quantum yield test data of NP-CDs

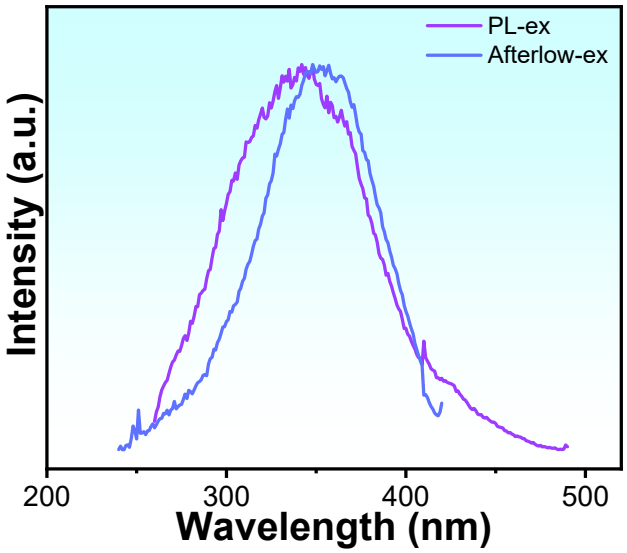

Fig. S2. Excitation spectra of the PL and Afterglow of NP-CDs.

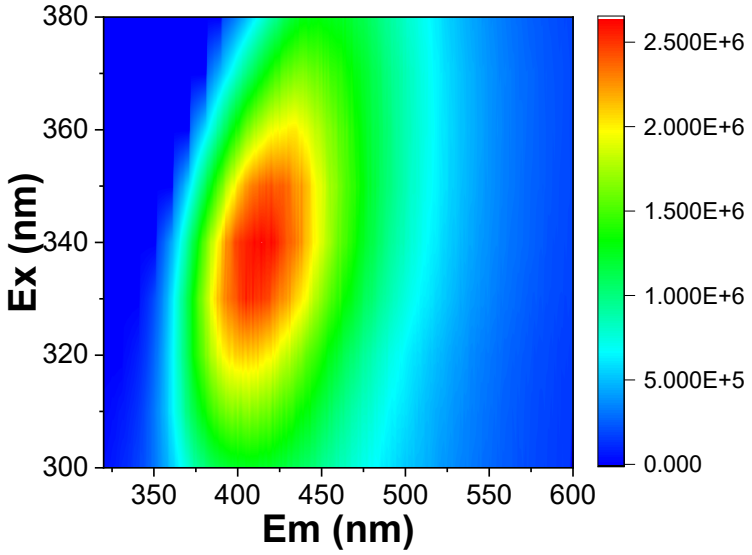

Fig. S3. PL 3D spectrum of NP-CDs.

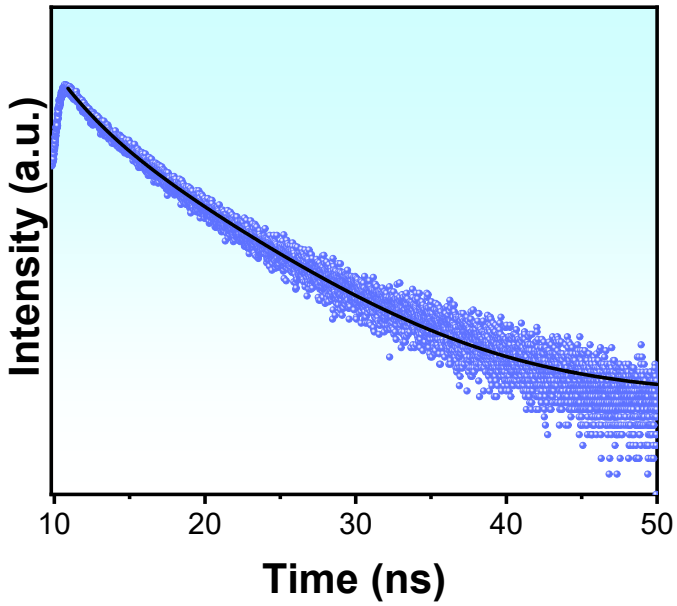

Fig. S4. FL decay spectrum of the NP-CDs.

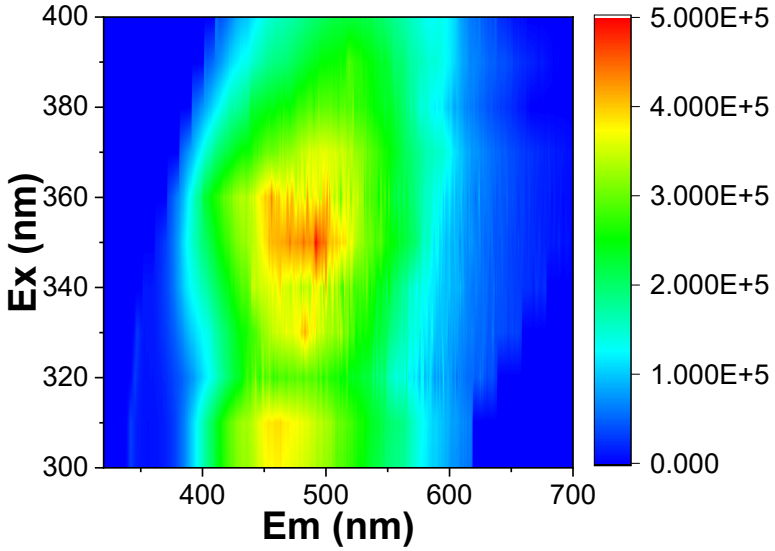

Fig. S5. Afterglow 3D spectrum of NP-CDs.

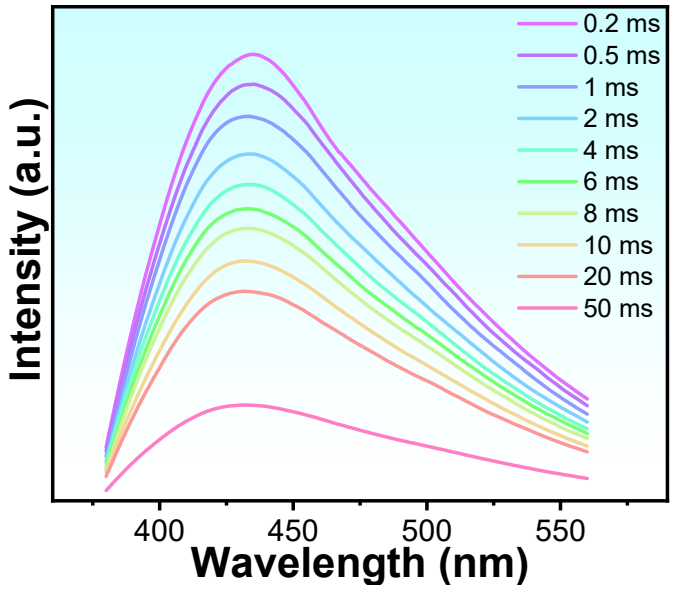

Fig. S6. The afterglow spectrum of NP-CDs under different gating times.

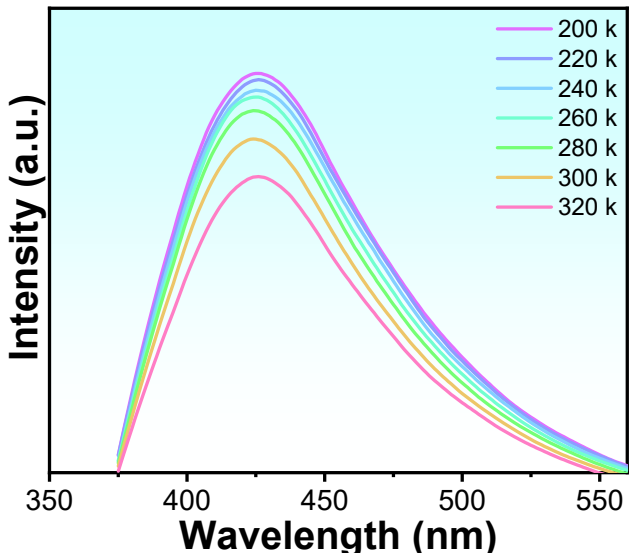

Fig. S7. PL spectra of NP-CDs at different temperatures.

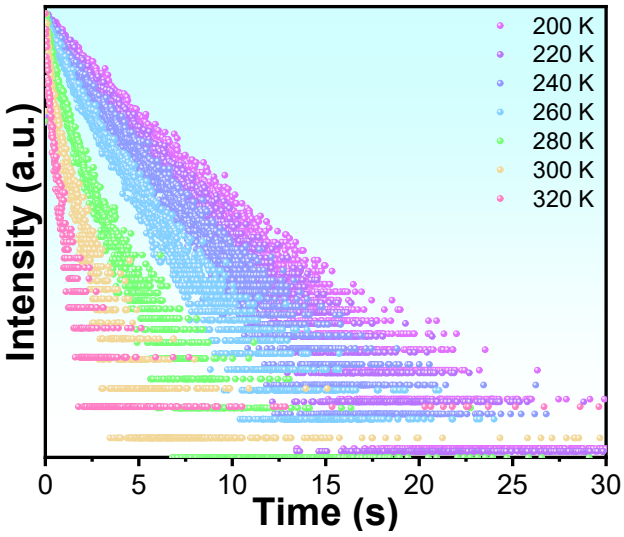

Fig. S8. Delayed fluorescence decay curves of NP-CDs at different temperatures under 437 nm.

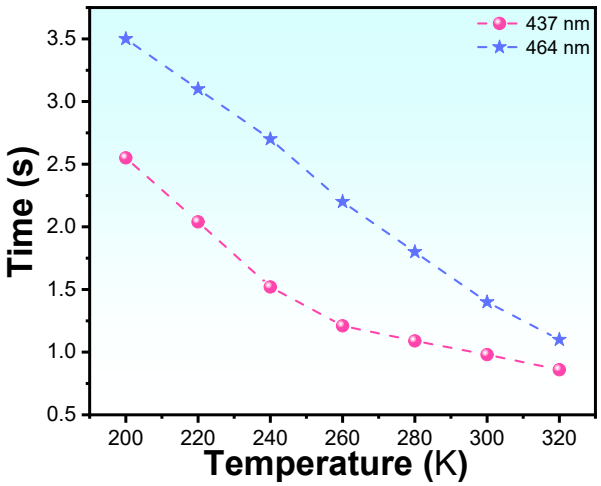

Fig. S9. The evolution of average lifetime of NP-CDs at 437nm and 464 nm varies with the detection temperature.

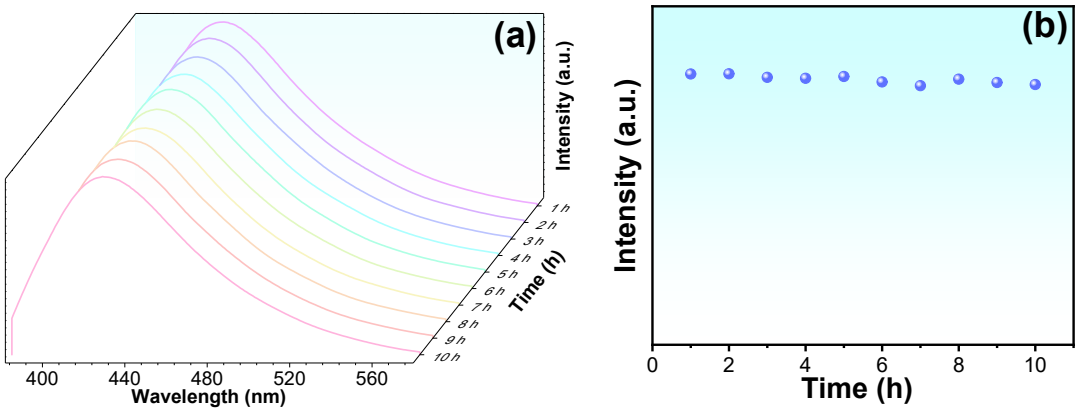

Fig. S10. The PL spectrum (a) and relative intensity (b) of NP-CDs under continuous UV irradiation for 10 hours.

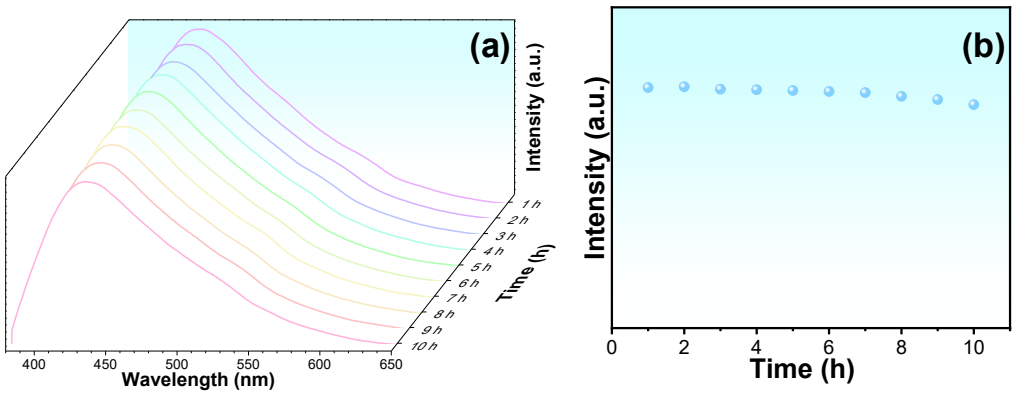

Fig. S11. The afterglow spectrum (a) and relative intensity (b) of NP-CDs under continuous UV irradiation for 10 hours.

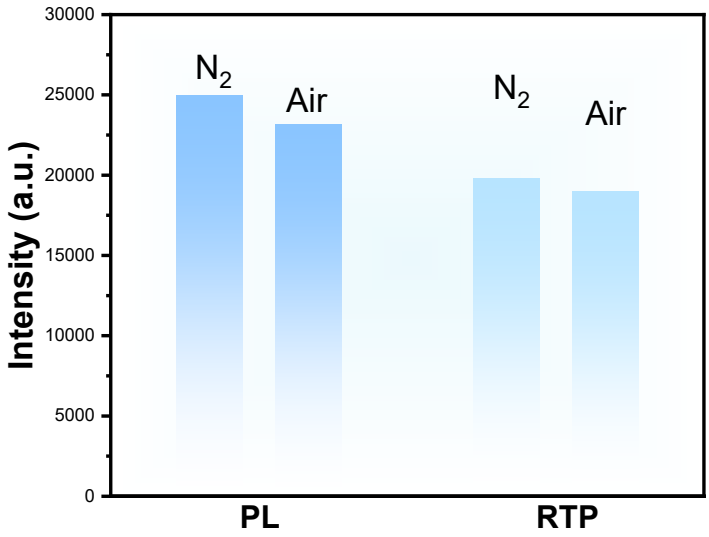

Fig. S12. The PL and afterglow intensity of the NP-CDs under different atmospheres.

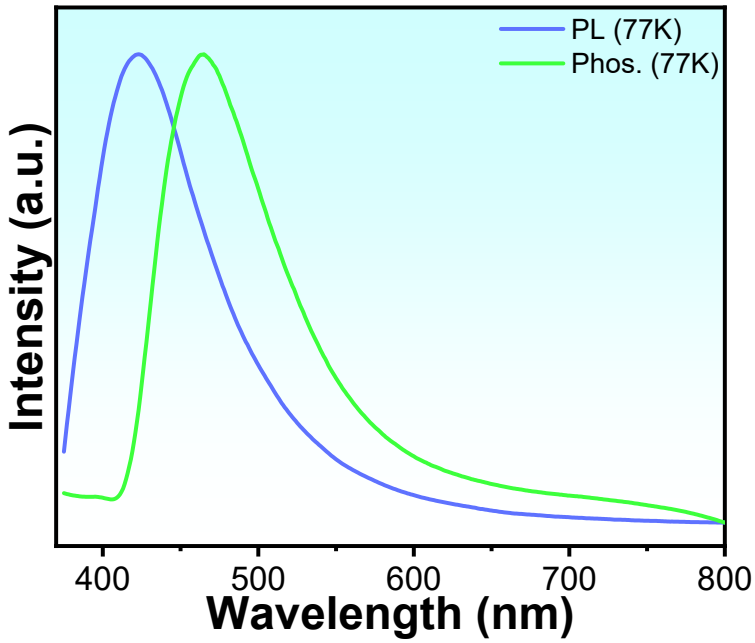

Fig. S13. PL and RTP spectra of the NP-CDs measured at 77 K upon excitation at 365 nm.

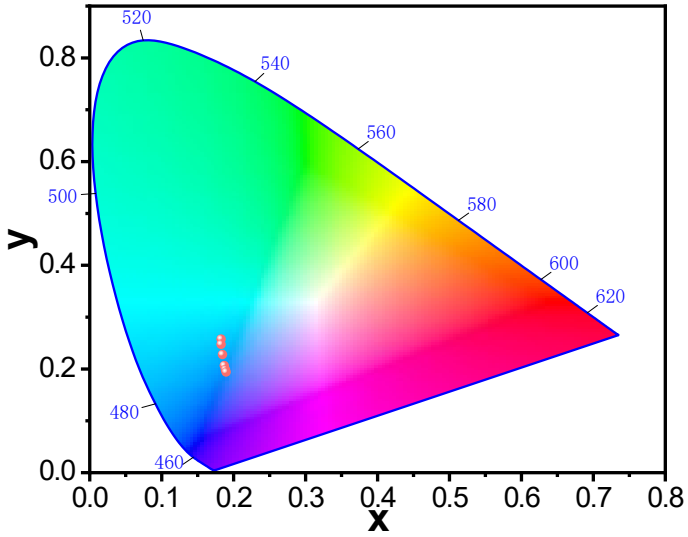

Fig. S14. CIE coordinate diagram of afterglow emissions from NP-CDs under different temperature conditions (200K-320K).

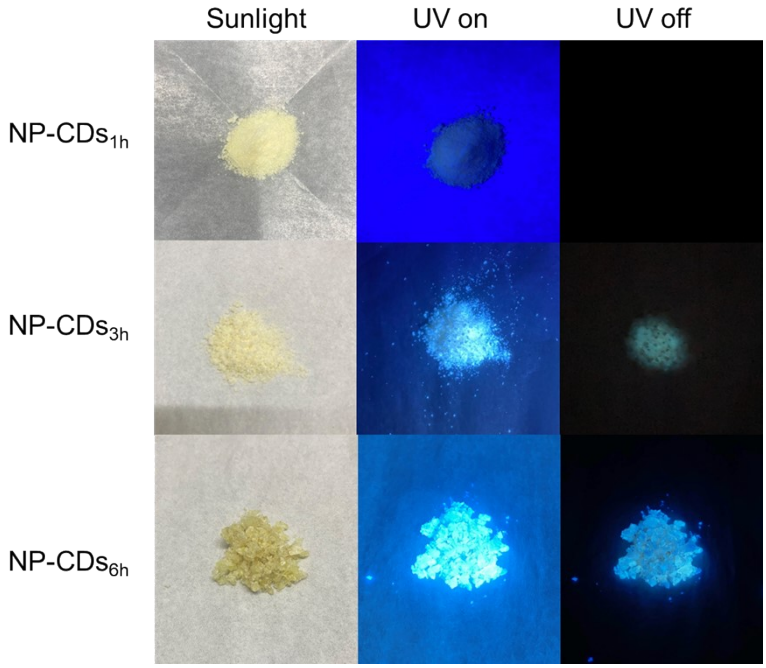

Fig. S15. Images of NP-CDs$_{1h}$, NP-CDs$_{3h}$, NP-CDs$_{6h}$ under sunlight, UV on, and UV off respectively.

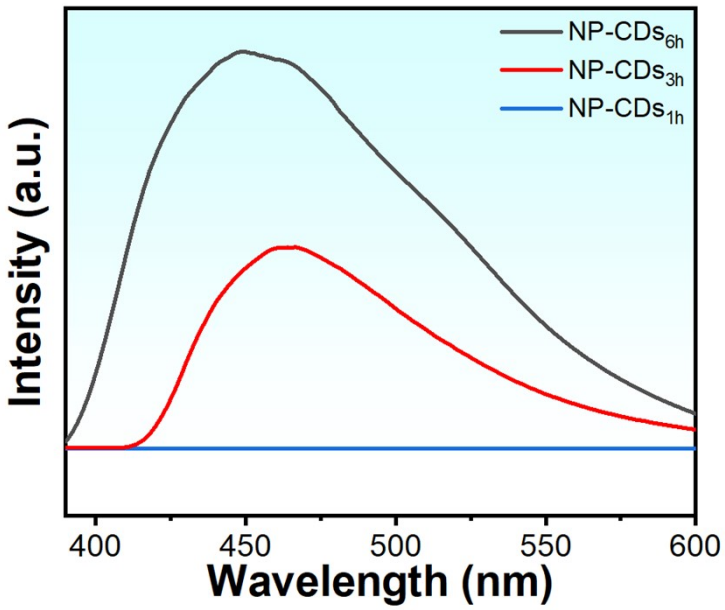

Fig. S16. Afterglow spectra of NP-CDs$_{1h}$, NP-CDs$_{3h}$, NP-CDs$_{6h}$ in vacuum.

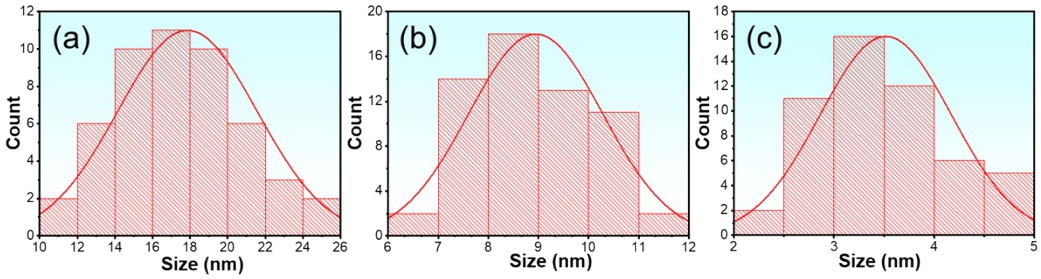

Fig. S17. The corresponding particle histogram of NP-CDs$_{1h}$, NP-CDs$_{3h}$, NP-CDs$_{6h}$.

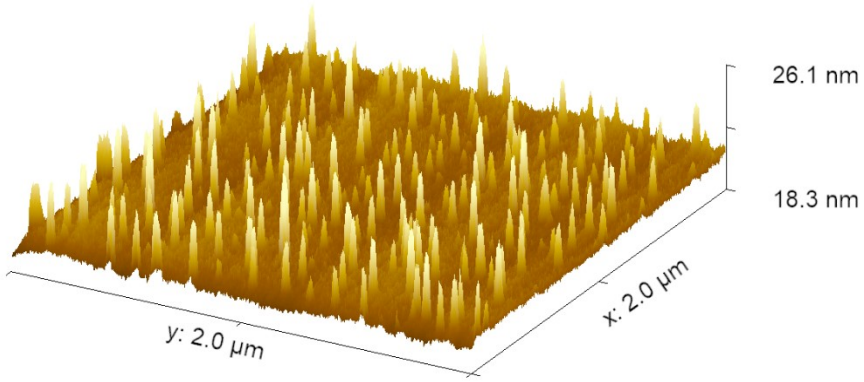

Fig. S18. 3D AFM images of NP-CDs$_{6h.}$

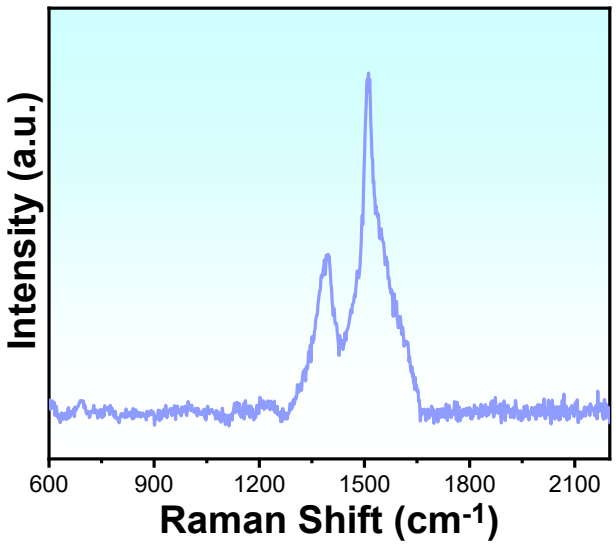

Fig. S19. Raman spectrum of the NP-CDs$_{6h}$.

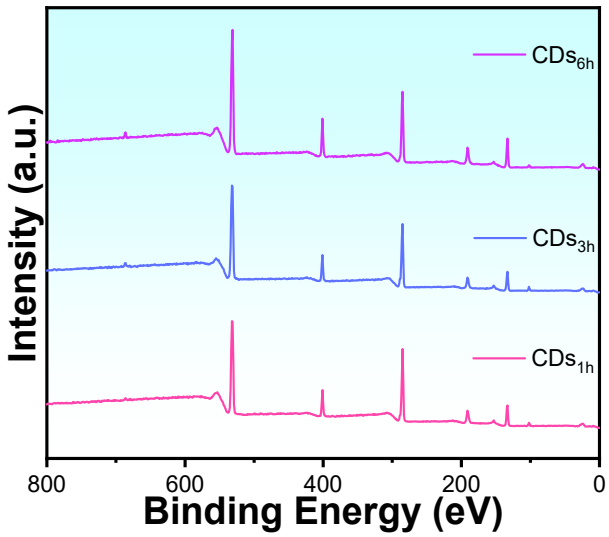

Fig. S20. XPS survey of the NP-CDs$_{1h}$ NP-CDs$_{3h}$ and NP-CDs$_{6h}$.

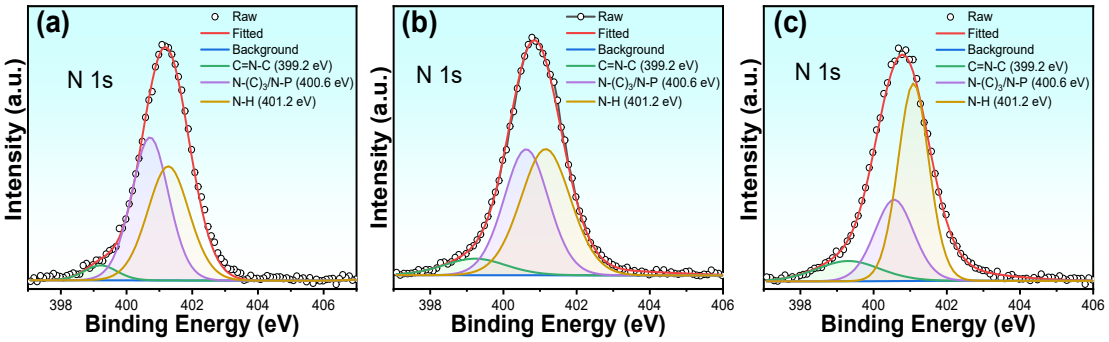

Fig. S21. High-resolution N 1s spectra of the NP-CDs$_{1h}$ NP-CDs$_{3h}$ and NP-CDs$_{6h}$.

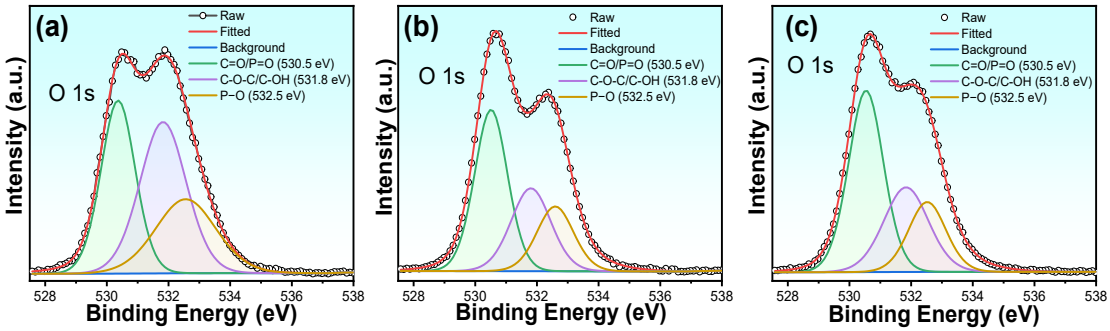

Fig. S22. High-resolution O 1s spectra of the NP-CDs$_{1h}$ NP-CDs$_{3h}$ and NP-CDs$_{6h}$.

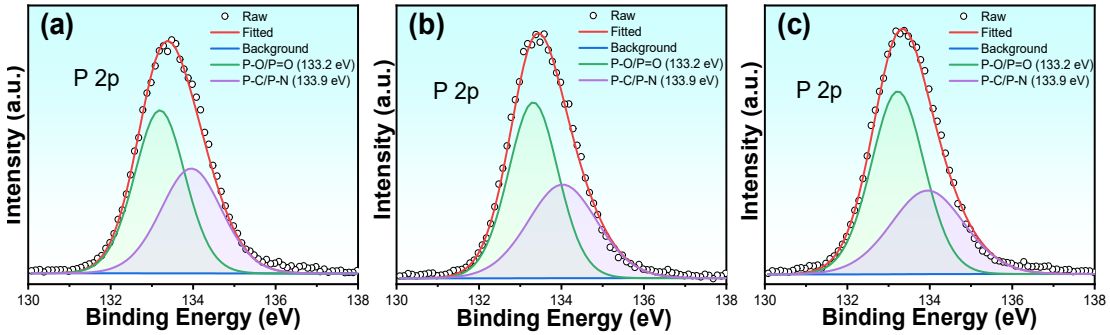

Fig. S23. High-resolution P 2p spectra of the NP-CDs$_{1h}$ NP-CDs$_{3h}$ and NP-CDs$_{6h}$.

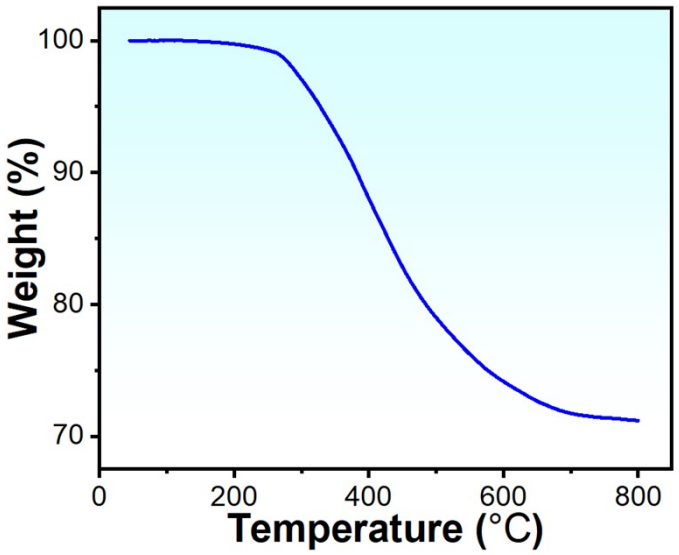

Fig. S24. TGA curve of the NP-CDs$_{6h}$.

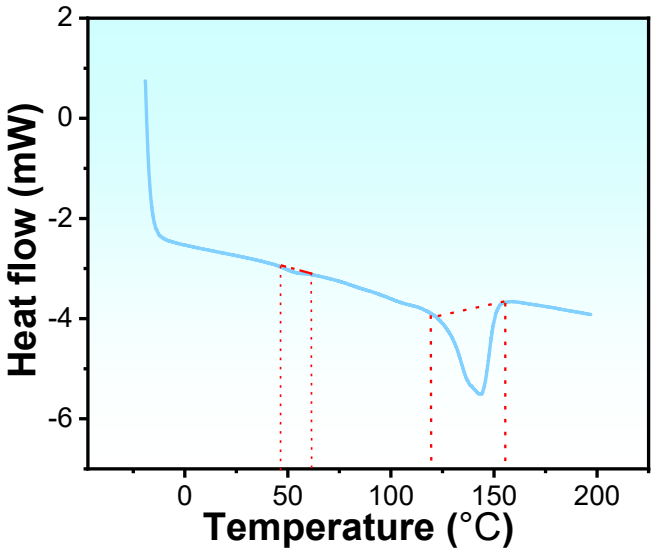

Fig. S25. DSC curve of the NP-CDs$_{6h}$.

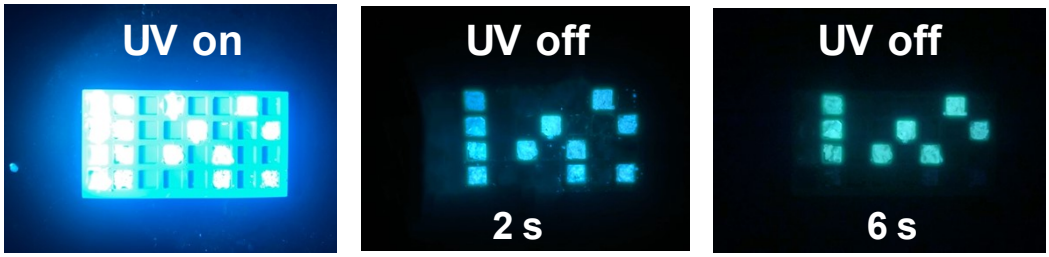

Fig. S26. Photographs of the dynamic evolution of the dot-matrix pattern based on models to give "BIT" decrypting information after ceasing 365 nm UV lamp.

Table S1 Summary of the current reported different RTP CDs.

Name	Em (nm)	QY (%)	Ref.
NP-CDs	458	64.70	This work
B-CDs300	462	50.17	[1]
B-CD	466	3.39	[2]
b-R-CDs	483	9.05	[3]
CB5-20	406	37.6	[4]
BA	456	0.82	[5]
MBA	415	45.30	[6]

Table S2 PL-decay lifetimes and fitting parameters of NP-CDs solution and powder.

Sample	τ_1 (ns)	B_1 (%)	τ_2 (ns)	B_2 (%)	τ_{avg} (ns)	x^2
Powder	3.426	42.61	8.614	57.39	6.403	0.999

Table S3 The phosphorescence decay lifetimes and fitting parameters of NP-CDs powder were measured at a wavelength of 458 nm across different temperatures.

Temperature (K)	τ_1 (ms)	B_1 (%)	τ_2 (ms)	B_2 (%)	τ_3 (ms)	B_3 (%)	τ_{avg} (s)	x^2
200	27.32	3.00	2863.29	12.69	3772.64	84.31	3.5	0.999
220	40.11	2.58	2672.69	18.77	3348.91	78.65	3.1	0.999
240	33.61	5.62	2364.72	20.86	2972.65	73.52	2.7	0.999
260	37.59	7.37	1679.98	22.85	2465.15	69.78	2.2	0.999
280	45.72	8.97	1209.72	25.72	2199.75	65.31	1.8	0.999
300	551.45	10.57	872.69	29.46	1792.78	59.97	1.4	0.999
320	7.55	9.92	586.32	30.21	1584.69	59.87	1.1	0.999

Table S4 The phosphorescence decay lifetimes and fitting parameters of NP-CDs powder were measured at a wavelength of 437 nm across different temperatures.

Temperature (K)	τ_1 (ms)	B_1 (%)	τ_2 (ms)	B_2 (%)	τ_3 (ms)	B_3 (%)	τ_{avg} (s)	x^2
200	290.93	8.6	1601.42	13.68	2972.63	77.72	2.55	0.999
220	300.41	9.32	1387.29	24.34	2518.15	66.34	2.04	0.999
240	256.62	12.54	1009.75	27.72	2060.56	59.74	1.52	0.999
260	206.72	11.64	1198.65	30.68	1402.21	57.68	1.21	0.999
280	194.52	10.17	986.79	34.52	1107.58	55.31	1.09	0.999
300	154.72	7.65	846.31	38.63	1194.63	53.72	0.98	0.999
320	109.65	7.15	759.98	44.23	1076.29	48.62	0.86	0.999

Table S5 Relative contents of different element in the NP-CDs_{1h}、NP-CDs_{3h} and NP-CDs_{6h}.

Sample	C 1s (%)	N 1s (%)	O 1s (%)	P 2p (%)
NP-CDs_{1h}	36.52	13.43	40.28	9.77
NP-CDs_{3h}	41.93	11.93	36.57	9.57
NP-CDs_{6h}	46.60	10.57	34.93	7.90

Reference

[1] Z. Song, Y. Shang, Q. Lou, J. Zhu, J. Hu, W. Xu, C. Li, X. Chen, K. Liu, C. Shan, X. Bai, *Adv. Mater*.,2022, **35**, 2207970.

[2] Y. Ding, X. Wang, M. Tang, H. Qiu, *Adv. Sci*., 2021, **9**, 2103833.

[3] Z. Ding, C. Shen, J. Han, G. Zheng, Q. Ni, R. Song, K. Liu, J. Zang, L. Dong, Q. Lou, C. Shan, Small, 2022, **19**, 2205916.

[4] J. Zhang, S. Xu, Z. Wang, P. Xue, W. Wang, L. Zhang, Y. Shi, W. Huang, R. Chen, *Angew. Chem. Int. Ed.*, 2021, **60**, 17094.

[5] H. Zheng, P. Cao, Y. Wang, X. Lu, P. Wu, *Angew. Chem. Int. Ed.*, 2021, **60**, 9500-9506

[6] Z. Zhang, Y. Shi, Y. Liu, Y. Xing, D. Yi, Z. Wang, D. Yan, *Chem. Eng. J.*, 2022, **442**, 136179.